Available online at www.sciencedirect.com
SCIENCE DIRECT®
Journal of Solid State Chemistry 178 (2005) 2934–2941
JOURNAL OF SOLID STATE CHEMISTRY
www.elsevier.com/locate/jssc

Crystal structure of $Ca_5Nb_5O_{17}$

J. Guevarra[a,*], S. van Smaalen[a], N. Rotiroti[a], C. Paulmann[b], F. Lichtenberg[c]

[a] *Lehrstuhl für Kristallographie, Universität Bayreuth, Universitätsstraße 30, D-95440 Bayreuth, Germany*
[b] *Mineralogisch-Petrographisches Institut, Universität Hamburg, Grindelalle 48, D-20146 Hamburg, Germany*
[c] *Institut für Physik, EKM, Experimentalphysik VI, Universität Augsburg, Universitätsstraße 1, D-86135 Augsburg, Germany*

Received 19 May 2005; received in revised form 1 July 2005; accepted 8 July 2005

Abstract

The crystal structure of $Ca_5Nb_5O_{17}$, an $n = 5$ member of the homologous series $A_nB_nO_{3n+2}$, at room temperature has been determined by single-crystal X-ray diffraction using synchrotron radiation with a CCD area detector. The structure is monoclinic with spacegroup $P2_1/c$ (b unique) and lattice parameters $a = 7.7494(3)$ Å, $b = 5.4928(1)$ Å, $c = 32.241(1)$ Å, and $\beta = 96.809(4)^\circ$. It consists of perovskite-like slabs of corner-sharing NbO_6 octahedra separated by an interslab region, where the octahedra on opposite sides of the gap do not share oxygen atoms resulting in an extra layer of oxygen atoms with respect to the ideal perovskite structure. The slabs are five octahedra wide. Ca atoms within the slabs occupy 12-fold coordinated sites whereas those at the borders show irregular coordination environments. The distortion of the octahedra increases from the center to the borders of the slabs. The computed valences for the Nb ions are very close to 5 at the borders while smaller values were obtained for sites in the middle of the slabs which suggests that the electrical conduction takes place predominantly in the middle of the slabs.

Keywords: X-ray diffraction; $A_nB_nO_{3n+2}$; Perovskite; Octahedra tilting; Pseudo-merohedral twinning; Bond valence sum

1. Introduction

Perovskite-related oxidic compounds of the series $A_nB_nO_{3n+2}$ ($A = \mathrm{Ca, Sr}$ or La and $B =$ Ti or Nb) with $n = 4, 4.33, 4.5, 5, 6$ and 7 have been the subject of much research because of their interesting electronic and dielectric properties [1–5]. Depending on the oxygen stoichiometry, these niobium- or titanium-based oxides exhibit different physical properties. The $n = 4$ insulators display ferroelectricity with very high transition temperatures. Some of the $n = 4.5$ and $n = 5$ electrical conductors show quasi-one-dimensional (1D) metallic behavior at high temperatures whereas at low temperatures there is a metal-to-semiconductor transition [1–5]. This transition is discussed in terms of a Peierls scenario but there are several open questions [2–5].

The crystal structures of compounds $A_nB_nO_{3n+2} = ABO_x$ ($x = 3 + 2/n$) are derived from the ABO_3 perovskite-type structure with slabs of vertex-sharing BO_6 octahedra separated by an interslab region. The octahedra on opposite sides of the interslab region do not share oxygen atoms thus leaving an extra layer of oxygen atoms with respect to the ideal perovskite structure. The crystal structure type is given by n which corresponds to the number of octahedral layers in the slab and can be tuned by adjusting the oxygen content. The ideal perovskite structure corresponds to the limiting value $n = \infty$. Non-integral values of n correspond to ordered sequences of octahedral slabs with different widths, e.g., $n = 4.5$ corresponds to alternating slabs four and five octahedra wide. The slabs are stacked along the [110] direction of the ideal perovskite structure (along $\mathbf{c}^*$ in the present study). Consecutive slabs of octahedra are shifted with respect to each other by half of the body diagonal of the octahedron. Furthermore, in the interlayer regions the octahedra do not share oxygen

*Corresponding author. Fax: +49 921 553770.
E-mail address: jonathan.guevarra@uni-bayreuth.de (J. Guevarra).

0022-4596/$ - see front matter © 2005 Elsevier Inc. All rights reserved.
doi:10.1016/j.jssc.2005.07.007

atoms, resulting in an irregular coordination of the A cations in these regions.

Diffraction studies on $Ca_n(Ti,Nb)_nO_{3n+2}$ series with $n = 4.5, 5,$ or 6 have demonstrated that these compounds have either an orthorhombic symmetry or a monoclinic symmetry, the latter giving rise to pseudo-merohedral twinning [6,7]. In particular for the compound $Ca_5(Nb_4Ti)O_{17}$ ($n = 5$), monoclinic symmetry was established with $P2_1$ and $P2_1/c$ as possible space-groups. Apparent orthorhombic symmetry, as revealed by precession photographs, occurs because of the relative shift of neighboring layers by $\mathbf{a}_p/2$, where a_p is the lattice constant of a hypothetical undistorted perovskite-type structure. Lattice parameters for this compound were reported as: $a \approx 2a_p$, $b \approx 2^{1/2}a_p$, $c \approx 2^{1/2}6a_p$. Their study, however, did not involve structure refinements and a crystal structure was not reported. More recently, single-crystal X-ray diffraction studies have been reported on a series of similar compounds, now involving complete structure refinements. These include $SrNbO_{3.4}$ ($n = 5$) [8], $Sr(Nb_{0.8}Ti_{0.2})O_{3.4}$ ($n = 5$) [9], $SrNbO_{3.5}$ ($n = 4$) [10], $LaTiO_{3.4}$ ($n = 5$) [11], $(Na_{0.2}\ Ca_{0.8})NbO_{3.4}$ ($n = 5$) [12], and $Ca(Nb_{0.76}Ti_{0.24})O_{3.33}$ ($n = 6$) [13].

A general description and classification of symmetries of the $A_nB_nO_{3n+2}$ type of compounds has been reported by Levin and Bendersky [14]. They discussed a classification scheme that relates the stacking sequences and octahedral tilt to the symmetry of these structures. They suggested that in most of these structures the displacive transition from a high-temperature untilted structure to a low-temperature tilted structure occurs in two stages: untilted $\rightarrow \mathbf{a}^+ \rightarrow \mathbf{a}^+\mathbf{b}$ or $\mathbf{a}^+\mathbf{c}$, with doubling of the a lattice parameter at the final transition. More recently a structural study by transmission electron microscopy on the $Sr_n(Nb,Ti)_nO_{3n+2}$ series with $n = 4, 4.5, 5, 6,$ and 7 has been published by Levin et al. [15]. These compounds were reported to undergo commensurate $\rightarrow$ incommensurate phase transitions at temperatures ranging from 150 to 250 °C, with the modulation vector close to $\mathbf{a}^*/2$. A lock-in phase to $\mathbf{a}^*/2$ was only found for the compound with $n = 5$, and the following sequence of phase transitions was established from high temperature to room temperature: *Immm*(*untilted*) $\rightarrow$ *Pmnn* $\rightarrow$ *incommensurate phase* $\rightarrow$ $P2_1/c$. The final monoclinic structure was found to have $a \approx 2a_p$ (7.7 Å).

In the present study we report the crystal structure of $Ca_5Nb_5O_{17}$ ($n = 5$) which is a diamagnetic, electrically conducting compound (formal valence $Nb^{4.8+}$, $4d^{0.2}$) [1]. The crystal structure is monoclinic, $P2_1/c$, with the existence of a pseudo-merohedral twinning. A two-fold superstructure along [100] was found. A detailed description of the deformation of NbO_6 octahedra at different positions in the slab and its possible relation to the electrical properties of the compound is given.

2. Experimental

Crystals of $Ca_5Nb_5O_{17}$ were prepared from $CaCO_3$, Nb_2O_5, and Nb as starting materials and by subsequent floating-zone melting in argon as reported by Lichtenberg et al. [1]. The actual composition determined by thermogravimetric oxidation was found to be $Ca_5Nb_5O_{17.05} = CaNbO_{3.41}$. This is within one standard uncertainty of the nominal composition since the accuracy of the oxygen content was found to be about 0.3% [1]. It was reported that for this compound the structure type ($n = 5$) remains unchanged in the homogeneity range $3.40 \leqslant x \leqslant 3.42$, as revealed by X-ray powder diffraction, transmission electron microscopy, and thermogravimetry [1].

Several crystals were prepared for X-ray diffraction by breaking them off a large aggregate and gluing them to glass fibers. Because of its layered structure, very thin plates of the sample were obtained by this method. The crystals were tested for quality on an MAR345 IP diffractometer and the better ones were subsequently tested on a Nonius MACH3 diffractometer with a rotating-anode generator using molybdenum radiation. Several good-quality single crystals were found, the best one having relatively sharp reflection profiles with a full-width at half-maximum (FWHM) less than 0.2° in ω-scans, which is still larger than the instrumental resolution of about 0.1° (Fig. 1). Omega scans for different psi values showed that the profiles for each reflection were almost the same, thus confirming the good quality of the crystal.

Lattice parameters were determined from the setting angles of 25 reflections, with $40.0° \leqslant 2\Theta \leqslant 52.2°$, in four orientations as measured on the Nonius MACH3 diffractometer using the SET4 centering routine [17] (Table 1). Owing to the weakness of the superstructure reflections (h = odd) and the long time required for data

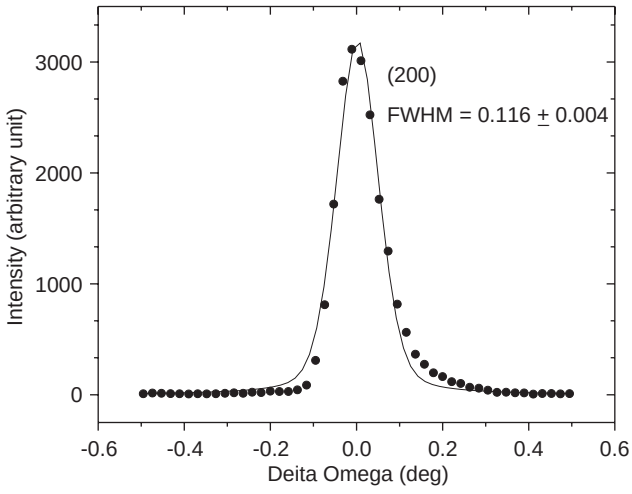

Fig. 1. Sample rocking curve for the 2 0 0 reflection. The data points are fitted by using the computer program Microcal Origin [16].

Table 1
Experimental details

Crystal data	
Chemical formula	$Ca_5Nb_5O_{17}$
Molecular weight	936.91
Cell setting, Spacegroup	Monoclinic, $P2_1/c$ (No. 14)
a, b, c (Å)	7.7494(3), 5.4928(1), 32.241(1)
β (°)	96.809(4)
V (Å^3), Z	1362.7(1), 4
D_{calc} (Mg/mm^3), μ (mm^{-1})	4.5653(3), 5.836
Crystal size (mm^3)	$0.13 \times 0.08 \times 0.03$
Crystal color, Shape	Dark-blue, irregular plate-like
Data collection	
Radiation	Synchrotron
Wavelength (Å)	0.7100(2)
Temperature (K)	295
Diffractometer	Huber Kappa Diffractometer
Detector	CCD: Bruker SMART1000
Range of h,k,l	$-11 \rightarrow 11, -8 \rightarrow 8, -52 \rightarrow 52$
Maximum 2θ	71.05°
No. of reflections (obs/all)	25839/31864
Criterion for observed	$I > 3\sigma$
No. of unique reflections (obs/all)	4719/5427
R_{int} (obs/all)	0.0352/0.0355
Absorption correction	Multi-scan(SADABS 2.03) [22]
Refinement	
Refinement on	F
Weighting scheme	$w = 1/[\sigma^2(\|F\|) + (0.01\|F\|)^2]$
$(\Delta/\sigma)_{max}$	0.001
No. of parameters	249
R_F (obs/all)	0.0247/0.0296
wR_{F^2} (obs/all)	0.0318/0.0330
Goodness of fit (obs/all)	1.76/1.70
Twinvol(II)	0.0272(3)
Extinction correction	Isotropic, Gaussian [23]
Extinction coefficient	0.014(2)
$\Delta\rho_{min}/\Delta\rho_{max}$ (e/Å^3)	−1.98/2.95

collection due to the large unit cell of the compound, measurements using the MACH3 diffractometer were deemed ineffective in producing the information necessary to carry out structure determination. Therefore an X-ray diffraction experiment at room temperature was carried out using synchrotron radiation at beamline F1 of Hasylab at DESY in Hamburg, Germany. The experiment used a Huber diffractometer with Kappa geometry and a CCD area detector (Bruker SMART 1000). Data collection was performed using the SMART (v.5.618) software [18]. A wavelength of $\lambda = 0.7100(2)$ Å was chosen in order to minimize absorption and to allow a reasonable portion of the reciprocal space to be measured. The detector was set to a distance of 60 mm from the crystal, while the fine-slicing technique was employed to collect the images with a step-size of 0.1° for omega scans and phi scans. The data collection was strategized using the computer program ASTRO (v.5.0.07) [19] for optimal coverage and redundancy in consideration of the coupled limits of the motors driving the circles of the diffractometer. A total of 16 runs were measured with detector offsets of 20° and 45° for measurement of the low-angle and high-angle reflections, respectively, plus an intermediate detector offset of 30° to complete the coverage. Exposure times per frame were 4 and 8 s, for the low-angle and high-angle measurements, respectively. A data coverage of 100% in the point group $2/m$ was achieved for a resolution of 0.67 Å with maximum 2Θ of 71.05°. The minimum and maximum redundancy were 1 and 17, respectively, with a mean of 8.0. The decay of the primary-beam intensity was corrected using SAPRO (v.1.5.50) [20]. Diffraction intensities were integrated using SAINT (v.6.2) [21]. An integration box with dimensions $1.1° \times 1.1° \times 0.5°$ was used for the integration using orientation matrices found with the SMART software. Refinement of the orientation matrix was performed during the integration procedure every 200–300 frames and global refinement of the cell parameters was done after each integration. Absorption correction and scaling were applied using SADABS (v.2.03) [22] with point symmetry $2/m$. SADABS relies on a sufficiently high redundancy of the data, as was indeed achieved (see above). Before parameter refinement in SADABS, $R_{int} = 0.0773$ and after parameter refinement, $R_{int} = 0.0364$.

The diffraction patterns reveal weak $h =$ odd reflections. Analysis of the systematic absence in the reflections using SIR2002 [24] led to $P2_1$ and $P2_1/c$ as possible spacegroups. Reflections at different psi-values were averaged together with symmetry-equivalent reflections (point group $2/m$) employing JANA2000 [25]. A good agreement with $R_{int} = 0.0352$ for 4719 unique observed reflections was obtained (Table 1). The diffraction pattern also shows an apparent orthorhombic symmetry. In fact, the transformation $\mathbf{a}_o = \mathbf{a}_m, \mathbf{b}_o = \mathbf{b}_m, \mathbf{c}_o = \mathbf{a}_m + \mathbf{2c}_m$ of the primitive monoclinic unit cell results in a B-centered unit cell that is orthorhombic within experimental resolution. Orthorhombic symmetry was considered by an additional run of SADABS employing point symmetry *mmm*. After parameter refinement, $R_{int} = 0.1010$ was obtained. Averaging in *mmm* led to $R_{int} = 0.0377$, slightly but clearly higher than R_{int} for Laue symmetry $2/m$. The deviation from orthorhombic symmetry is mainly due to the superlattice formation: $R_{int} = 0.179$ for reflections $h =$ odd, while $R_{int} = 0.036$ for reflections with $h =$ even. In the case of $2/m$, $R_{int} = 0.045$ for reflections $h =$ odd, while $R_{int} = 0.034$ for reflections with $h =$ even.

The structure of $LaTiO_{3.41}$ was used as starting model [11]. The structure was refined using JANA2000. Initial refinements in $P2_1/c$ converged at $R_F = 0.0318$ and $wR_{F^2} = 0.0542$ for observed reflections. However, there were reflections violating the systematic absence for the c-glide plane. An improved fit to the diffraction data was obtained by the introduction of pseudo-merohedral twinning, assuming a twin law corresponding to a two-fold axis along **a**, resulting in the superposition of

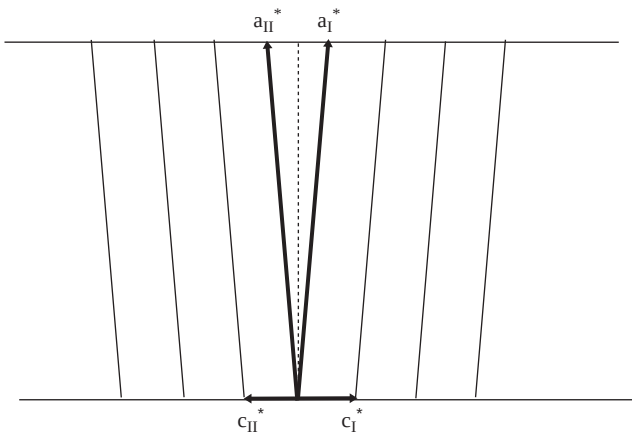

Fig. 2. Orientation of the two twin domains in reciprocal space in the case of pseudo-merohedral twinning of the crystal: $(h\,k\,l)_{\mathrm{I}} = (h\,{-}k\,{-}(h+l))_{\mathrm{II}}$.

reflections $(h\,k\,l)_{\mathrm{I}}$ and $(h\,-\,k{-}(h+l))_{\mathrm{II}}$ of the respective twin domains (Fig. 2). In a transmission electron microscope study Levin and Bendersky [14] have reported the presence of twin-related monoclinic variants for the $n = 5$ type of the $Sr_n(Nb,Ti)_nO_{3n+2}$ series while complete structure refinements using this twin model have also been reported in similar perovskite-related compounds [12,13]. Using this twin model, reflections of type $(h0l)$ where $h =$ odd and $l =$ odd which were found to violate the *c*-glide plane are now accounted for by the second twin domain ($h =$ odd, $0, l =$ even). The final refinement with all atoms refined anisotropically converged at $R_{\mathrm{F}} = 0.0247$ and $wR_{\mathrm{F}^2} = 0.0318$ (Table 1). Further details of the crystal structure investigation(s) can be obtained from the Fachinformationszentrum Karlsruhe, 76344 Eggenstein-Leopoldshafen, Germany, (fax: (49) 7247-808-666; e-mail: crysdata@fiz.karlsruhe.de) on quoting the depository number CSD 415450.

3. Discussion

The accurate crystal structure of $Ca_5Nb_5O_{17}$ has been determined from single-crystal X-ray diffraction. Only an accurate crystal structure provides quantitatively correct information on the tilting and deformations of the octahedra at different sites in the slabs. As we show below, this information provides an insight into the structural and physical properties of the compound.

Fractional atomic coordinates and equivalent isotropic displacement parameters are summarized in Table 2. Projections of the structure along the **a** * and **b** * directions are shown in Fig. 3. Successive slabs of octahedra stacked along the **c**-axis are shown to be shifted by $\mathbf{a}/2$. The tilt pattern of the NbO_6 octahedra with respect to the untilted orthorhombic structure is

Table 2
Fractional atomic coordinates and equivalent isotropic atomic displacement parameters (Å^2) of $Ca_5Nb_5O_{17}$

Atom[a]	*x*	*y*	*z*	U_{eq}
Ca1	0.25442(4)	0.50567(6)	0.00643(7)	0.0063(1)
Ca2	0.29938(4)	0.99595(6)	0.09547(8)	0.0045(0)
Ca3	0.79172(5)	0.00012(7)	0.08310(1)	0.0088(1)
Ca4	0.31644(5)	0.52001(7)	0.20820(1)	0.0103(1)
Ca5	0.13777(4)	0.08703(6)	0.27833(1)	0.0053(0)
Nb1	0.5	0	0	0.0018(0)
Nb2	0	0	0	0.0017(0)
Nb3	0.54317(2)	0.50348(2)	0.09191(0)	0.0021(0)
Nb4	0.04897(2)	0.50462(2)	0.09114(0)	0.0019(0)
Nb5	0.08599(2)	0.02596(3)	0.17709(0)	0.0027(0)
Nb6	0.59517(2)	0.03031(3)	0.17815(0)	0.0027(0)
O1	0.5559(1)	0.2934(2)	0.0343(0)	0.0057(3)
O2	0.9784(1)	0.2942(2)	0.0344(0)	0.0062(3)
O3	0.4867(1)	0.7895(2)	0.0514(0)	0.0056(3)
O4	0.0650(1)	0.7900(2)	0.0512(0)	0.0059(3)
O5	0.0772(1)	0.2952(2)	0.2103(0)	0.0065(3)
O6	0.6365(1)	0.3189(2)	0.2032(0)	0.0077(3)
O7	0.1352(1)	0.8046(2)	0.2198(0)	0.0053(3)
O8	0.5930(1)	0.8238(2)	0.2242(0)	0.0060(3)
O9	0.0350(1)	0.1869(2)	0.1183(0)	0.0053(3)
O10	0.5827(1)	0.1836(2)	0.1175(0)	0.0045(3)
O11	0.3358(1)	0.0900(2)	0.1693(0)	0.0064(3)
O12	0.1649(1)	0.4280(2)	0.3309(0)	0.0064(3)
O13	0.1247(1)	0.7050(2)	0.1354(0)	0.0068(3)
O14	0.5115(1)	0.7019(2)	0.1366(0)	0.0067(3)
O15	0.7941(1)	0.5631(2)	0.0888(0)	0.0084(3)
O16	0.2897(1)	0.4140(2)	0.0792(0)	0.0043(3)
O17	0.7517(1)	0.9206(2)	0.0039(0)	0.0064(3)

[a]All atoms are in general positions except Nb1 and Nb2, which are in special positions with multiplicity 0.5.

described in Fig. 4. It is clear that the octahedra exhibit tilting about the **a**-axis (about $\mathbf{a}^*$ in the present study) (Fig. 4a). This kind of tilt is described as an $\mathbf{a}^+$ tilt as the octahedra *along* the rotation axis are tilted in the same sense [14]. Neighboring octahedra along the **a**-axis also exhibit antiphase tilts *about* the **c**-axis (about $\mathbf{c}^*$ in the present study), i.e., consecutive octahedra are rotated clockwise and anticlockwise along the **a**-axis (Fig. 4b). It was reported that the effect of a **c** tilt leads to a doubling of the *a* lattice parameter [14,26]. Thus, the tilt pattern observed in the present case is a combination of tilts, $\mathbf{a}^+\mathbf{c}$. Such tilting modes have also been registered for the $n = 5$ member of the $Sr_n(Nb,Ti)_nO_{3n+2}$ series and have been attributed to the sequence of symmetry transformation: *Immm*(*untilted*) $\rightarrow$ *Pmnn* $\rightarrow$ *incommensurate phase* $\rightarrow$ $P2_1/c$ [15]. The topology of the structure and the tilt system of the octahedra for the present compound indeed corresponds to that expected for a structural motif composed of an odd number of layers of octahedra. A similar topology has been reported for other perovskite-related $n = 5$-type compounds [11,12].

The interatomic distances show that the Ca atoms at the borders of the slabs (Ca4,Ca5) are less than 12-fold coordinated by oxygen, while the coordination of Ca

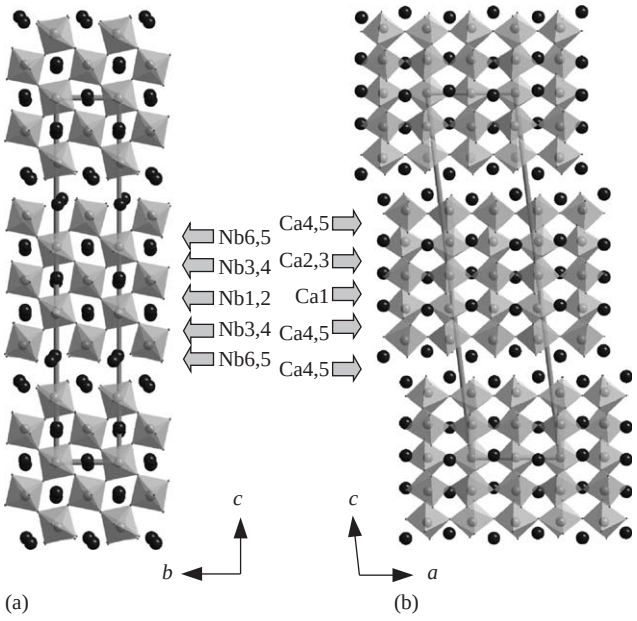

Fig. 3. Projections of the structure of $Ca_5Nb_5O_{17}$ along (a) the **a*** and (b) the **b*** directions. Large dark spheres represent Ca atoms while the NbO_6 octahedra are outlined.

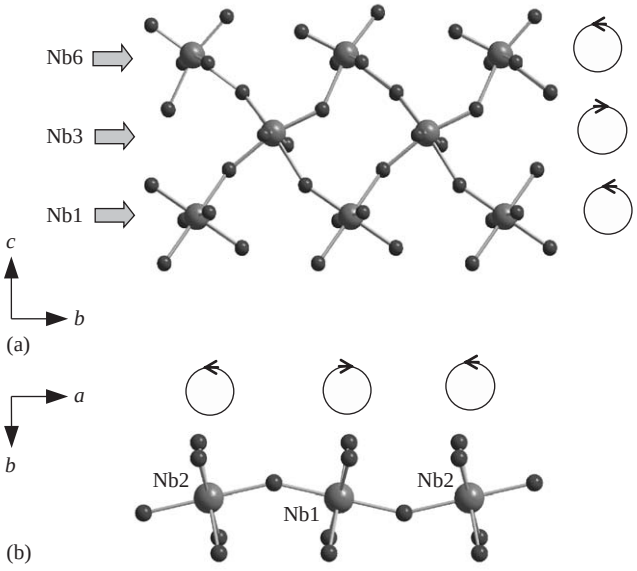

Fig. 4. NbO_6 octahedra tilting about (a) **a*** and (b) **c*** in $Ca_5Nb_5O_{17}$. Also shown are the sense of tilt of the octahedra.

atoms embedded within the slabs (Ca1,Ca2,Ca3) can be described by a distorted cubooctahedron, as it would be expected for a perovskite-type structure, in agreement with coordinations in similar layered perovskites [9–13]. Ca4 is coordinated by 10 oxygen atoms with Ca–O bond distances ranging from 2.411(1) to 3.369(1) Å, while Ca5 has seven coordinating oxygen atoms with bond distances from 2.309(1) to 2.518(1) Å. Ca1, Ca2, and

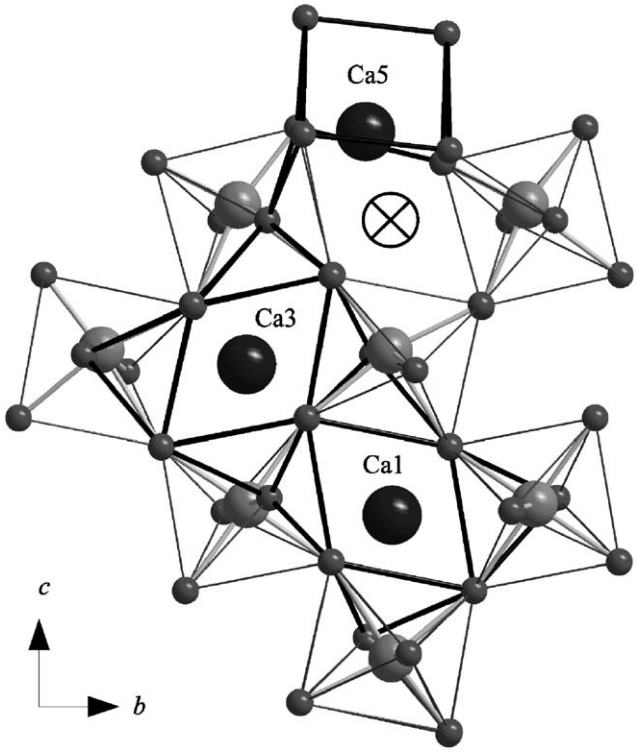

Fig. 5. Coordination of Ca atoms. Ca1 is in the middle of the slabs while Ca5 is at the border. The dark lines between the O atoms are only a means to clarify the coordination geometries and do not represent chemical bonds. The symbol ⊗ marks the position that Ca5 would occupy in a 12-fold coordination.

Ca3 are bonded to 12 oxygen atoms with bond lengths ranging from 2.302(1) to 3.403(1) Å. As shown in Fig. 5, Ca5, which is located at the borders of the slabs, is displaced out of the center of the coordinating polyhedra towards the neighboring slab, while Ca1 and Ca3, which are embedded within the slabs, exhibit a distorted cubooctahedron coordination. The deviation of Ca5 from the center of its coordinating polyhedra toward the interlayer regions is consistent with local charge neutrality as there are excess oxygen atoms in these regions. For the Ca atoms within the slabs, the distortion follows from the slight shift of the Ca atoms from the centers of the coordinating cubooctahedra.

The distortions of the NbO_6 octahedra can be described in terms of the Nb–O bond lengths and the O–Nb–O bond angles. Fig. 6 shows that different Nb sites have different ranges of Nb–O bond lengths. It is clear that the spread in bond lengths around Nb and the deviation of each Nb–O distance from the mean value per Nb site, which is about 2 Å, increase from the center to the borders of the slabs. This variation in bond lengths represents a variation of distortion of NbO_6 octahedra. A measure for the size of the octahedral distortion is the distortion index, $[\max(d[\mathrm{Nb-O}]) - \min(d[\mathrm{Nb-O}])]/\mathrm{ave}(d[\mathrm{Nb-O}])$ [1], which is large at the

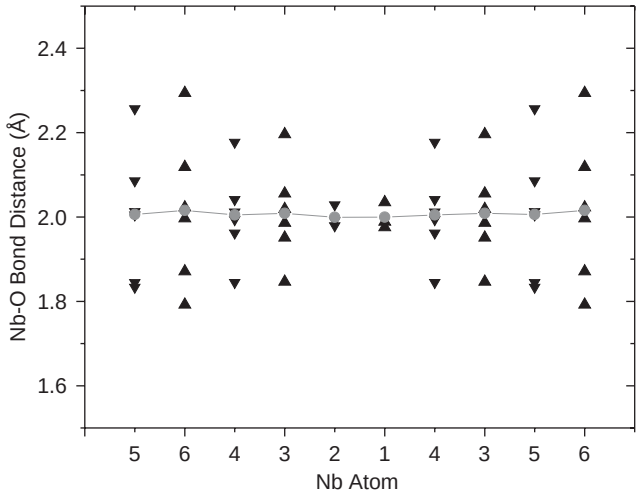

Fig. 6. Bond distances between different Nb atoms and their coordinating O atoms. The Nb atoms are arranged such that the center of the horizontal axis of the graph corresponds to the center of the slab. The symbol ▲ corresponds to Nb atoms on one row along the **c**-axis while the symbol ▼ refers to a second row displaced by **a**/2. The symbol ● denotes the mean Nb–O distance.

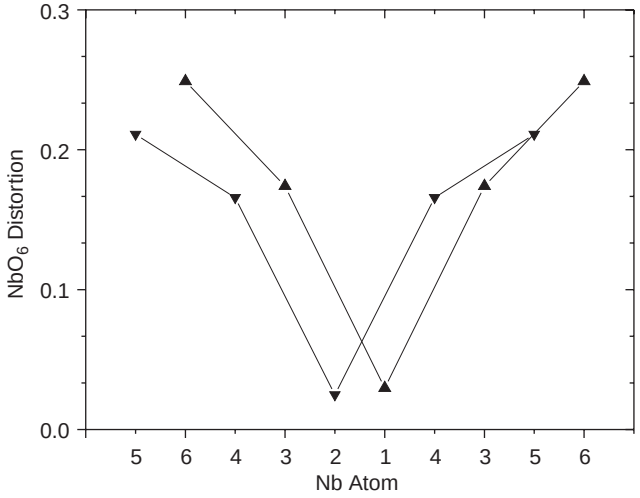

Fig. 7. NbO_6 octahedral distortion. The Nb atoms are arranged such that the center of the horizontal axis of the graph corresponds to the center of the slab. The symbol ▲ corresponds to Nb atoms on one row along the **c**-axis while the symbol ▼ refers to a second row displaced by **a**/2.

borders and small in the middle of the slabs (Fig. 7). The large distortion of octahedra at the borders of the slabs (Nb5,Nb6) can be attributed to the elongation of some Nb–O distances (e.g., d[Nb5−O13] = 2.256(1) Å and d[Nb6−O14] = 2.293(1) Å). This is also reflected by the relatively large displacement parameters of Nb5 and Nb6 as compared to other Nb sites in the slabs, which manifests a stretching of the octahedra into the interlayer regions. With respect to the mean O–Nb–O bond angles, there are no significant differences among the different Nb sites (Table 3). The standard uncertainty of the mean, however, increases from the center to the borders of the slab. Thus, the distortion of the NbO_6 octahedra in terms of bond-length and bond-angle grows from the center to the borders of the slabs in agreement with previous studies on related layered perovskites [9–13].

Bond-valence sums [27] were computed for all different Nb sites in the slab (Fig. 8). The valence of Nb is close to 5.0 v.u.(valence units) [4.953(1)–4.984(1) v.u.] at the borders of the slabs, and it decreases towards the center of the slabs. The smaller valence at the center of the slabs [4.730(1)–4.733(1) v.u.] indicates that the extra electrons in the 4d orbitals of Nb are most probably accommodated at Nb sites in the middle of the slabs. This implies that the electrical conduction in this compound takes place probably in the middle of the slab where the NbO_6 octahedra are least distorted. Angle-resolved photoemission studies (ARPES) and band-structure calculations on $Sr_5Nb_5O_{17}$ ($n = 5$) have concluded that the predominant contribution to the occupied electron density of states at the Fermi energy comes from the least distorted octahedra which are

Table 3
Mean O–Nb–O bond angles (deg) in $Ca_5Nb_5O_{17}$

O–Nb1–O	90.00 (47)
O–Nb2–O	90.00 (46)
O–Nb3–O	89.64 (200)
O–Nb4–O	89.70 (184)
O–Nb5–O	89.69 (210)
O–Nb6–O	89.57 (222)

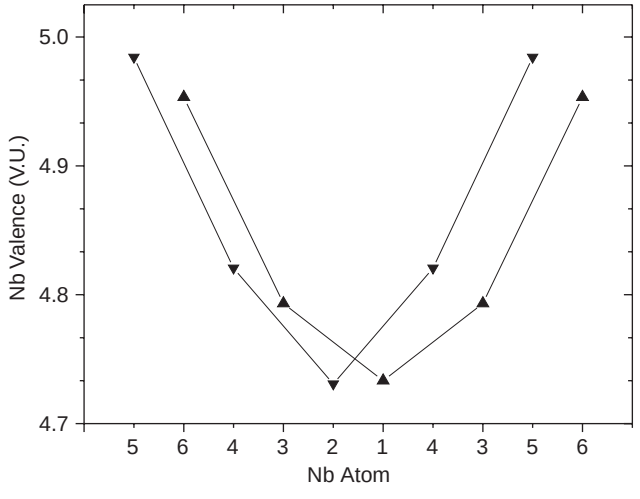

Fig. 8. Nb valence for the different Nb sites in the octahedral slab. The Nb atoms are arranged such that the center of the horizontal axis of the graph corresponds to the center of the slab. The symbol ▲ corresponds to Nb atoms on one row along the **c**-axis while the symbol ▼ refers to a second row displaced by **a**/2.

found in the middle of the slabs [2–4]. In the insulator of $Ca(Nb, Ti)O_{3.33}$ type ($n = 6$) with exclusively Nb^{5+} and Ti^{4+}, there is a similar trend of charge distribution as indicated by the experimentally determined site occupancies of the *B* cations, Nb and Ti [13]. In this compound, the borders of the slab are filled almost entirely by Nb^{5+} while at the center of the slab, the largest amount of substitution of Nb^{5+} by Ti^{4+} is found. On the other hand, in $Ca_5Nb_5O_{17}$ the borders of the slabs are also occupied by Nb^{5+} but in the center of the slab the Nb ions have a smaller fractional charge. It is interesting to note that on the basis of a crystal structure analysis, one is able to obtain information about the charge distribution of the *B* cations along the slabs of the octahedra.

The unit cell volume of monoclinic $Ca_5Nb_5O_{17}$ is approximately twice as large as that of $Sr_5Nb_5O_{17}$ which was reported to have orthorhombic symmetry [8]. With respect to the distortions of the NbO_6 octahedra, there are no fundamental differences between the two structures for similar Nb sites (Table 4). The differences between the two structures are in the tilting of the NbO_6 octahedra and concomitantly in the coordinations of the Ca and Sr atoms, respectively. Fig. 9 shows the coordination of Ca2 in $Ca_5Nb_5O_{17}$ and Sr3 in $Sr_5Nb_5O_{17}$; both are located intermediate between the center and the borders of their respective slabs. While in $Sr_5Nb_5O_{17}$ Sr3 occupies the center of the coordinating cubooctahedron, Ca2 in $Ca_5Nb_5O_{17}$ is shifted away from the center of the coordinating polyhedra. The shift of Ca2 is accompanied by rotations of the octahedra as allowed by the lower monoclinic symmetry found for $Ca_5Nb_5O_{17}$. The superstructure, which was not found in $Sr_5Nb_5O_{17}$, is manifested in an unusually high valence of Ca2 (2.236(1) v.u.) in $Ca_5Nb_5O_{17}$ which suggests a residual compressive strain. This local strain, in turn, is relieved by a commensurate modulation of the structure leading to a two-fold superstructure along [100], as presently found for $Ca_5Nb_5O_{17}$. The different sizes and strengths of interactions of Ca versus Sr may result in the superstructure to appear in $Ca_5Nb_5O_{17}$ and not to appear in $Sr_5Nb_5O_{17}$. But it may also be that a similar superstructure does indeed exist in $Sr_5Nb_5O_{17}$, and that this was not detected [8]. An investigation is in progress to clarify this issue.

Table 4
Range of Nb–O bond distances (Å) and mean O–Nb–O bond angles (°) in $Sr_5Nb_5O_{17}$ [8] [a]

Nb1–O	1.973 (3)–2.034 (3)
Nb3–O	1.842 (3)–2.170 (3)
Nb2–O	1.815 (3)–2.280 (3)
O–Nb1–O	90.00 (36)
O–Nb3–O	89.73 (176)
O–Nb2–O	89.63 (201)

[a]The Nb atoms are arranged from the center (Nb1) to the border (Nb2) of the slabs.

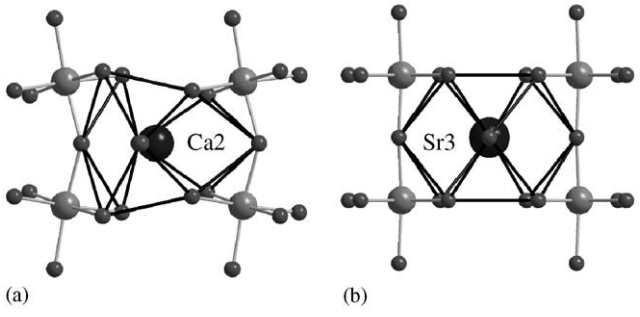

Fig. 9. Coordination of (a) Ca2 in $Ca_5Nb_5O_{17}$ viewed along **c***, and (b) Sr3 in $Sr_5Nb_5O_{17}$ viewed along **a***. The view directions relative to the topology are the same in both cases; only the unit-cell settings are different.

4. Conclusions

The crystal structure of $Ca_5Nb_5O_{17}$ at room temperature has been successfully determined by single-crystal X-ray diffraction with synchrotron radiation. This compound is an $n = 5$ member of the series $A_nB_nO_{3n+2}$ (A = Ca, Sr or La and B = Ti or Nb). It consists of perovskite-like slabs, which are five NbO_6 octahedra wide separated by an interslab region, where the octahedra on opposite sides of the gap do not share oxygen atoms resulting in an extra layer of oxygen atoms with respect to the ideal perovskite structure. The topology of the structure and the tilt system of the octahedra corresponds to that expected for a structural motif with $n = 5$ layers of octahedra. The structure is monoclinic ($P2_1/c$) with a two-fold superstructure along [100]. The Ca atoms near the borders of the slabs have irregular coordination geometry with seven coordinating oxygen atoms, while the coordination of Ca atoms within the slabs can be described by a distorted cubooctahedron. The NbO_6 octahedra at the center of the slabs are much less distorted than those at the borders of the slabs. The computed valences for Nb suggest that the electrical conduction in this compound takes place predominantly in the middle of the slabs.

Acknowledgments

Beam time at beamline F1 of Hasylab at DESY (Hamburg, Germany) was obtained under the proposal number II-03-036. JG acknowledges the Deutscher Akademischer Austauschdienst (DAAD) for financial support. FL acknowledges financial support by the BMBF (Project No. 13N6918A)

References

[1] F. Lichtenberg, A. Herrnberger, K. Wiedenmann, J. Mannhart, Progr. Solid State Chem. 29 (2001) 1–70.

[2] C.A. Kuntscher, S. Gerhold, N. Nücker, T. Cummins, D. Lu, S. Schuppler, C. Gopinath, F. Lichtenberg, J. Mannhart, K.P. Bohnen, Phy. Rev. B 61 (3) (2000) 1876–1883.

[3] C.A. Kuntscher, S. Schuppler, P. Haas, B. Gorshunov, M. Dressel, M. Grioni, F. Lichtenberg, A. Herrnberger, F. Mayr, J. Mannhart, Phys. Rev. Lett. 89 (23) (2002) 236403.

[4] C.A. Kuntscher, S. Schuppler, P. Haas, B. Gorshunov, M. Dressel, M. Grioni, F. Lichtenberg, Phy. Rev. B 70 (24) (2004) 245123.

[5] J. Weber, C. Kegler, N. Büttgen, H. Krug von Nidda, A. Loidl, F. Lichtenberg, Phys. Rev. B 64 (23) (2001) 235414.

[6] M. Nanot, F. Queyroux, J. Gilles, J. Solid State Chem. 28 (1979) 137–147.

[7] M. Nanot, F. Queyroux, J. Gilles, in: R. Metselaar, H. Heijliger, J. Schonman (Eds.), Crystallochemistry of New Ferroelectric Compounds. Studies in Inorganic Chemistry, vol. 3, Elsevier, Amsterdam, 1983, pp. 623–626.

[8] S.C. Abrahams, H.W. Schmalle, T. Williams, A. Reller, F. Lichtenberg, D. Widmer, J. Bednorz, R. Spreiter, C. Bosshard, P. Günter, Acta Crystallogr. B 54 (1998) 399–416.

[9] A. Drews, W. Wong-Ng, R. Roth, T. Vanderah, Mater. Res. Bull. 31 (1996) 153–162.

[10] P. Daniels, R. Tamazyan, C.A. Kuntscher, M. Dressel, F. Lichtenberg, S. van Smaalen, Acta Crystallogr. B 58 (2002) 970–976.

[11] P. Daniels, S. van Smaalen, F. Lichtenberg, Acta Crystallogr. C 59 (2003) i15–i17.

[12] F. Zuniga, J. Darriet, Acta Crystallogr. C 59 (2003) i18–i20.

[13] J. Guevarra, S. van Smaalen, P. Daniels, N. Rotiroti, F. Lichtenberg, Z. Kristallogr. 220 (2005) 19–24.

[14] I. Levin, L. Bendersky, Acta Crystallogr. B 55 (1999) 853–866.

[15] I. Levin, L. Bendersky, T.A. Vanderah, Philos. Mag. A 80 (2000) 411–445.

[16] Microcal Software, Inc., Microcal Origin Software Reference Manual v.5.0, Northampton, MA, USA, 1997.

[17] Enraf-Nonius, CAD-4 Software, v.5.0, Enraf-Nonius, Delft, The Netherlands, 1989.

[18] Bruker, SMART for Windows NT and IRIX Software, v.5.0, Bruker AXS, Madison, USA, 1998.

[19] Bruker, ASTRO for Windows NT Software, v.5.0.07, Bruker AXS, Madison, USA, 1998.

[20] C. Paulmann, SAPRO for Windows NT Software, v.1.5.50, University of Hamburg, Hamburg, Germany, 2002.

[21] Bruker, SAINT, v.6.2. Program for the Integration of Intensities from Diffraction Images, Bruker AXS GmbH, Karlsruhe, Germany, 2000.

[22] G.M. Sheldrick, SADABS, v.2.03, Bruker Area Detector Absorption and other Corrections, University of Göttingen, Göttingen, Germany, 2002.

[23] P. Becker, P. Coppens, Acta Crystallogr. A 55 (1974) 129–153.

[24] M. Burla, M. Camalli, B. Carrozzini, G. Cascarano, C. Giacovazzo, P.G.R. Spagna, J. Appl. Crystallogr. 36 (2003) 1103.

[25] V. Petricek, M. Dusek, L. Palatinus, The Crystallographic Computing System JANA2000, Institute of Physics, Praha, Czech Republic, 2000.

[26] A.M. Glazer, Acta Crystallogr. A 31 (1975) 756–762.

[27] N. Brese, M. O'Keeffe, Acta Crystallogr. B 47 (1991) 192–197.